# Two-dimensional infrared spectroscopy of isotope-diluted ice Ih

Fivos Perakis, Susanne Widmer, and Peter Hamm

Citation: The Journal of Chemical Physics **134**, 204505 (2011); doi: 10.1063/1.3592561
View online: http://dx.doi.org/10.1063/1.3592561
View Table of Contents: http://scitation.aip.org/content/aip/journal/jcp/134/20?ver=pdfcov
Published by the AIP Publishing

# Two-dimensional infrared spectroscopy of isotope-diluted ice Ih

Fivos Perakis, Susanne Widmer, and Peter Hamm[a)]
*Physikalisch-Chemisches Institut, Universität Zürich, Winterthurerstrasse 190, CH-8057 Zürich, Switzerland*

(Received 28 March 2011; accepted 27 April 2011; published online 24 May 2011)

We present experimental 2D IR spectra of isotope diluted ice Ih (i.e., the OH stretch mode of HOD in $D_2O$ and the OD stretch mode of HOD in $H_2O$) at T = 80 K. The main spectral features are the extremely broad 1-2 excited state transition, much broader than the corresponding 0-1 ground-state transition, as well as the presence of quantum beats. We do not observe any inhomogeneous broadening that might be expected due to proton disorder in ice Ih. Complementary, we perform simulations in the framework of the Lippincott-Schroeder model, which qualitatively reproduce the experimental observations. We conclude that the origin of the observed line shape features is the coupling of the OH-vibrational coordinate with crystal phonons and explain the beatings as a coherent oscillation of the O···O hydrogen bond degree of freedom. © *2011 American Institute of Physics*. [doi:10.1063/1.3592561]

## I. INTRODUCTION

Water research attracts scientists from a variety of disciplines, ranging from biology, where it bounds to proteins and other biological macromolecules,[1] to astronomical observations,[2] such as its presence in carbon-rich stars.[3] Surprisingly, due to the strong hydrogen bonding nature of the water molecule which allows the formation of complex three dimensional hydrogen bonded motifs, the structure of the macroscopic liquid is still under debate.[4,5] It has been proposed that clusters of molecules occur, featuring tetrahedral molecular coordination,[6–10] in ways similar to that of the crystalline phase. In total 15 different crystalline phases of ice have been identified[11–13] as well as a variety of amorphous states.[14] One of the intriguing variations among the crystalline forms is that in some cases protons are randomly distributed in an otherwise regular oxygen lattice, following the ice rules.[15–17] Ice Ih, one of these disordered forms, is the stable crystalline ice under ambient pressure within the temperature range of 273 K to 72 K. Lower in temperature lies its proton ordered counterpart, ice XI.[18–21] Proton disorder is interesting from a theoretical point of view, considering the possible impact it has to the phonon and exciton dynamics of ice Ih.[22,23]

Neutron scattering provides a wealth of information on internal and external phonons of ice, since it is not subject to selection rules and reveals the density of states beyond the $k = 0$ phonons.[24–27] Furthermore, the linear IR and Raman spectra of ice Ih have been investigated throughout the whole frequency range.[28–34] Nonlinear spectroscopic studies such as pump-probe, hole-burning, photon-echo or 2D IR spectroscopy, on the other hand, remained much more scarce. In particular, the nonlinear infrared spectroscopy of the OH stretch vibration (or correspondingly the OD stretch vibration) is of interest, since the local molecular environment directly affects its frequency, line shape and dynamics.[35,36] The OH or OD stretch frequency is a sensitive probe of the hydrogen bond strength, that is, the stronger it is hydrogen bonded, the more red-shifted is its vibrational transition. To simplify the problem, one often investigates isotope diluted water, i.e., HOD in either $H_2O$ or $D_2O$. Isotope dilution spatially isolates the vibration from other resonant modes, so the excitation remains local and senses the local environment. The additional information obtained from nonlinear over linear spectroscopy concern the couplings between the various degrees of freedom of ice, as well as the contribution of disorder, due to the sensitivity of nonlinear spectroscopy in distinguishing homogeneous from inhomogeneous broadening.[37] Previous nonlinear spectroscopic studies of ice have resolved the vibrational dynamics of ice Ih using hole burning[38] and two-color mid IR pump-probe spectroscopy.[39] The temperature dependence of the vibrational lifetime has been explored,[40] its spectral features,[38,39] its dilution-dependence as well as its anisotropy[41] and the dynamics of ice in reverse micelles.[42]

One intriguing observation of previous pump-probe experiments were the extreme asymmetry in linewidth between the 0-1 and 1-2 transitions of the OH vibrator of $HOD/D_2O$.[38,39] The 1-2 transition, which is reached only in a nonlinear experiment, has an exceptionally broad linewidth of $\approx$350 $cm^{-1}$, comparable with that of liquid water, while that of the 0-1 transition is much narrower with $\approx$50 $cm^{-1}$.[39] It is generally assumed that the broad linewidth observed in liquid water reflects the large inhomogeneity in hydrogen bonding, contrary to the much narrower linewidth expected in ice, where disorder surely is less, despite the proton disorder discussed above. Along these lines, Bakker and co-workers concluded[39] that the additional broadening of the 1-2 transition must be due to lifetime broadening (corresponding to a $\approx$15 fs vibrational lifetime). They identified a Fermi resonance with the HOD bending mode at $\approx$1470 $cm^{-1}$ as the only conceivable source for such a fast de-excitation of the second excited state of the OH vibration. We will show though that this explanation is at least incomplete.

In the present paper, we discuss 2D IR experiments of isotope diluted ice Ih. The experiments are performed with higher time resolution than previous pump-probe

a)Electronic mail: phamm@pci.uzh.ch.

 

experiments, enabling us to detect quantum beats which we assign to strong anharmonic coupling to longitudinal acoustic phonons. Furthermore, the 2D IR measurement resolves the pump-frequency (in contrary to pump-probe spectroscopy), permitting discrimination between homogeneous and inhomogeneous broadening of the OH stretching mode. The latter would reflect inhomogeneity due to proton disorder, which however is not detectable. Finally, we perform experiments on both the OH vibration of HOD in $D_2O$ and the OD vibration of HOD in $H_2O$. Also the 1-2 transition of the OD vibration of HOD in $H_2O$ is significantly broader than the corresponding 0-1 transition, albeit not quite as much as for the OH vibration in HOD/$D_2O$. With this observation we argue that there must be other mechanisms responsible for the broadening of the 1-2 transition, possibly in addition to the suggested Fermi resonance,[39] since the OD vibration is no longer in resonance with the second overtone of the HOD bending mode. We show that a full non-adiabatic treatment of the Lippincott-Schroeder potential, which has been widely used to explain spectroscopic and structural features of hydrogen-bonded crystals,[43,44] can qualitatively explain all experimental observations.

## II. MATERIAL AND METHODS

### A. Experimental methods

A commercial Ti:sapphire oscillator and chirped pulse amplifier delivers ultrafast 800 nm pulses, of energy 1 mJ and repetition rate of 1 kHz. A homebuilt optical parametric amplifier (OPA)[45] is used to generate 1.8 $\mu$J tunable compressed mid-IR pulses of ≈65 fs duration (estimated by an interferometric autocorrelation measurement[46]) with a bandwidth of 250 $cm^{-1}$. As a central frequency we use 2420 $cm^{-1}$ for the OD stretch and 3280 $cm^{-1}$ for the OH stretch. For the 2D measurements, we used a Fourier transform 2D IR setup in pump-probe geometry.[47,48] The data acquisition is performed with a fast scanning routine, described in detail elsewhere.[48] Furthermore, the use of a wobbling brewster window makes it possible to measure highly scattering samples, like the ones presented here.[49]

We measure 14 population times between 50 fs and 1 ps at parallel $\langle ZZZZ\rangle$ polarization geometry. All measurement are taken at $T = 80K$ using a nitrogen cooled cryostat, making sure that we remain within the stable phase boundaries of ice Ih.[18–21] Purging with $N_2$ is necessary due to $CO_2$ absorption in the OD stretch frequency range. Our samples consist of 2.5% $D_2O$ in triple distilled and filtered $H_2O$ for probing the OD stretch and of 2.5% $H_2O$ in $D_2O$ for the OH stretch. The samples were enclosed between two $CaF_2$ windows, with a thin layer of vacuum grease and no spacer, yielding an effective thickness of ≈3 $\mu$m, in order to achieve the desired optical density.

### B. Theoretical methods

We explain the experimental results in the framework of the Lippincott-Schroeder model[43,44] (see theory section for a discussion of the validity and limitations of the model). For a better comparison with Bakker's work, we use the same functional form [Eq. (4) below] and parameters as Refs. 39, 50, and 51, i.e., $D_{Ia} = 38750\,cm^{-1}$, $D_{Ib} = 25000\,cm^{-1}$, $D_{II} = 2000\,cm^{-1}$, $n_{Ia} = 10\,Å^{-1}$, $n_{Ib} = 16.5\,Å^{-1}$, $n_{II} = 2.9\,Å^{-1}$, $r_0 = 0.97$ Å, and $R_0 = 2.88$Å. We note that other authors have used different functional forms for $V_{II}$ and different parameters.[43,44,52–54] The detailed outcome of the calculation does depend on these parameters, as such we stress that we do *not* consider the results to be quantitative. We will nevertheless see that the Lippincott-Schroeder potential can qualitatively reproduce the 2D IR response.

The kinetic energy operator was assumed to decouple for the two degrees of freedom, with an effective mass of $\mu_{OH} = 1$ for the OH vibration (or $\mu_{OD} = 2$ for the OD vibration, respectively), and $\mu_{O\cdots O} = 9$ for the O···O hydrogen bond coordinate (i.e., two waters with mass 18 oscillating against each other). We solved the problem on two levels: first, in the usual adiabatic treatment which is justified by the fact that the OH-vibration is about one order of magnitude higher in frequency than the O···O vibration; second, on a numerically exact level by solving the 2D vibrational Schrödinger problem, which implicitly includes all non-adiabatic couplings between the various $\nu_{OH}$ states. In both cases, we used a *sinc*-function DVR basis in cartesian coordinates[55] on a properly centered grid with a step size 0.07 Å in the $r_{OH}$-direction and 0.04 Å in the $R_{O\cdots O}$-direction (with these parameters, the relevant bound eigenstates are converged).

2D IR spectra were calculated from the vibrational eigenstates using diagrammatic perturbation theory.[37,56] To that end, the response functions of bleach ($R_{bl}$), stimulated emission ($R_{se}$), and excited state absorption ($R_{ex}$) have been calculated for both rephasing ($re$) and non-rephasing ($nr$) pathways:

$$R_{bl,re} = \sum_{i_1,j_0,k_1} \mu_{0,i_1}\mu_{i_1,j_0}\mu_{j_0,k_1}\mu_{k_1,0} \cdot e^{i(+\omega_{i_1}t_1+\omega_{j_0}t_2-(\omega_{k_1}-\omega_{j_0})t_3)}e^{-(t_1+t_3)/T_2}, \quad (1)$$

$$R_{bl,nr} = \sum_{i_1,j_0,k_1} \mu_{0,i_1}\mu_{i_1,j_0}\mu_{0,k_1}\mu_{k_1,j_0} \cdot e^{i(-\omega_{i_1}t_1-\omega_{j_0}t_2-\omega_{k_1}t_3)}e^{-(t_1+t_3)/T_2},$$

$$R_{se,re} = \sum_{i_1,j_1,k_0} \mu_{0,j_1}\mu_{0,i_1}\mu_{j_1,k_0}\mu_{i_1,k_0} \cdot e^{i(+\omega_{j_1}t_1-(\omega_{i_1}-\omega_{j_1})t_2-(\omega_{i_1}-\omega_{k_0})t_3)}e^{-(t_1+t_3)/T_2},$$

$$R_{se,nr} = \sum_{i_1,j_1,k_0} \mu_{0,i_1}\mu_{0,j_1}\mu_{j_1,k_0}\mu_{i_1,k_0} \cdot e^{i(-\omega_{i_1}t_1-(\omega_{i_1}-\omega_{j_1})t_2-(\omega_{i_1}-\omega_{k_0})t_3)}e^{-(t_1+t_3)/T_2},$$

$$R_{ex,re} = \sum_{i_1,j_1,k_2} \mu_{0,j_1}\mu_{0,i_1}\mu_{i_1,k_2}\mu_{k_2,j_1} \cdot e^{i(+\omega_{j_1}t_1-(\omega_{i_1}-\omega_{j_1})t_2-(\omega_{k_2}-\omega_{j_1})t_3)}e^{-(t_1+t_3)/T_2},$$

$$R_{ex,nr} = \sum_{i_1,j_1,k_2} \mu_{0,i_1}\mu_{0,j_1}\mu_{i_1,k_2}\mu_{k_2,j_1} \cdot e^{i(-\omega_{i_1}t_1-(\omega_{i_1}-\omega_{j_1})t_2-(\omega_{k_2}-\omega_{j_1})t_3)}e^{-(t_1+t_3)/T_2}.$$

The summation indexes $j_0, k_0$ run over all states in the $\nu_{OH} = 0$ manifold, $i_1, j_1$ in the $\nu_{OH} = 1$ manifold, and $k_2$ in the $\nu_{OH} = 2$ manifold. In the adiabatic calculation, the assignment of an eigenstate to one of these manifolds is given by construct, and the transition dipoles were calculated from the corresponding Franck-Condon factors. In the full 2D non-adiabatic calculation, this assignment is no longer clear-cut since strong mode mixing occurs. We therefore assigned states by their frequency ordering as well as through their connectivity by the transition dipole, which was computed as $\mu_{ij} = \langle \phi_i | r_{OH} | \phi_j \rangle$ (assuming that it is the polar OH group that gives rise to the oscillator strength). We assumed a low-temperature limit, so all pathways start from the overall ground state (with the chosen set of parameters for the Lippincot-Schroeder model, the first excited state with one quantum in the O···O coordinate lies at 405 $cm^{-1}$, so it will not be excited at the experimental temperature of 80 K. The same is still true when taking into account that this set of parameters over-estimates the O···O by a factor 2-3). The response functions were exponentially damped with a time constant of $T_2 = 50$ fs during the coherence times $t_1$ and $t_3$ for the OH vibration of HOD/$D_2O$ (and $T_2 = 300$ fs for the OD vibration of HOD/$H_2O$), effectively convoluting a 2D-stick spectrum with 2D Lorentzians with 200 $cm^{-1}$ (30 $cm^{-1}$) FWHM spectral width. No phenomenological damping factor was included for the population time $t_2$, so its dephasing (see Fig. 8 below) represents the inherent time-evolution of the wavefunction. The incoherent pump-probe spectra in Fig. 5 were calculated omitting all coherence terms during the population time $t_2$ (i.e., restricting the sums in $R_{bl}$ to $j_0 = 0$ and to $i_1 = j_1$ in $R_{se}$ or $R_{ex}$). This procedure mimics a double-resonance spectrum with spectrally narrow pump and probe pulses.

## III. EXPERIMENTAL RESULTS

To set the stage, we show in Fig. 1 the linear absorption spectra of isotope diluted ice Ih, which agree with previously measured spectra.[34] Two different isotopic mixtures have been measured: (a) the OH stretch of HOD/$D_2O$ and (b) the OD stretch of HOD/$H_2O$. The broad background distribution underlying the OD stretch [Fig. 1(b)] is the libration-bend combination mode of the $H_2O$ surrounding molecules. The OH stretch of ice Ih is more narrow and red-shifted compared to that of liquid water. The spectral narrowing reflects the much smaller variability of local structural motives around the OH or OD chromophore in the crystalline phase, despite the existence of proton disorder. Furthermore, the shift to lower frequencies indicates an average stronger hydrogen bonding environment,[57] which occurs already by cooling liquid water to lower temperatures.[36] In contrary, the libration-bend combination mode of the $H_2O$ [Fig. 1(b)] appears blue-shifted for the ice phase in comparison to the liquid.[58]

A selection of 2D IR spectra of the OH stretch vibration of HOD/$D_2O$ at $T = 80K$ is shown in Fig. 2, upper row, for population times $t_2$ varied between 100 fs and 1 ps. By convention, the horizontal axis is the probe frequency and the vertical the pump frequency. The signal intensity decreases as a function of population time $t_2$ due to vibrational relaxation (this effect is normalized out in Fig. 2 to facilitate a better comparison of the 2D IR line shape). The on-diagonal blue lobe (0-1 transition) is associated with ground state processes, such as bleach and stimulated emission. The red lobe (1-2 transition) is attributed to excited state absorption of the stretch vibration. In agreement with previous hole-burning[38] and pump-probe experiments,[39] the 1-2 transition is significantly broader than the corresponding 0-1 transition. This asymmetry is very pronounced for the OH stretch vibration in HOD/$D_2O$ (Fig. 2, upper row), but is also present for the OD stretch vibration in HOD/$H_2O$ (Fig. 2, lower row). The common dephasing theories used to describe 2D IR lineshapes[37,56] assume that fluctuations of the environment affect the 0-1 and the 1-2 transitions in a highly correlated manner, in which case they are expected to be equally broad. On the other hand, the vibrational relaxation ($T_1$) contribution to dephasing may affect the two transitions differently, which is the explanation put forward by Bakker and co-workers.[39] However, the observation of the asymmetry for both the OH and the OD stretch vibration challenges the explanation of Ref. 39 that a Fermi resonance with the HOD bending mode is responsible for lifetime broadening of the 1-2 transition. While the second overtone of the HOD bending mode at 1470 $cm^{-1}$ is indeed resonant with the 1-2 transition of the OH stretch vibration, this is no longer the case for the OD stretch vibration.

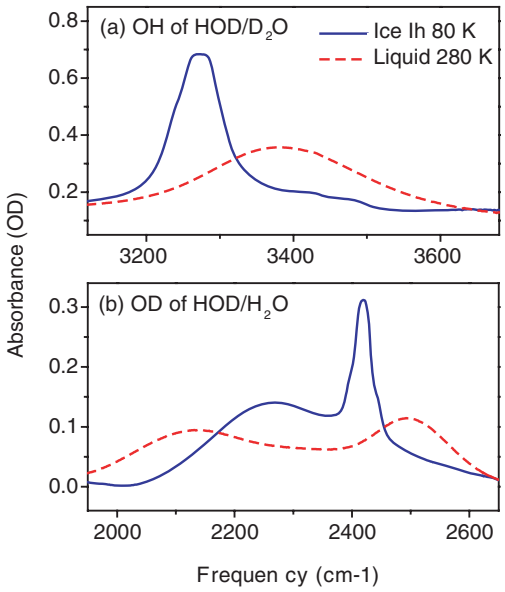


FIG. 1. Linear absorption spectra of the (a) OH stretch mode of HOD/ $D_2O$ and the (b) OD stretch mode of HOD/ $H_2O$. The spectra of liquid water (red dashed line) appear blue-shifted and much broader than that of ice Ih (blue solid line).

As a second piece of information extracted from the 2D IR spectra, we turn to the question of inhomogeneous broadening. We observe very little substructure in the 0-1 transition (indicated in Fig. 2 by the green square in the $t_2 = 200$ fs of OH of HOD/$D_2O$), apart from which the 2D IR lineshapes are hardly tilted along the diagonal in neither of the isotopomers. Such a tilt, which is observed for example for liquid water,[59–62] would reflect a correlation between pump and probe frequency, i.e., would reflect an inhomogeneity

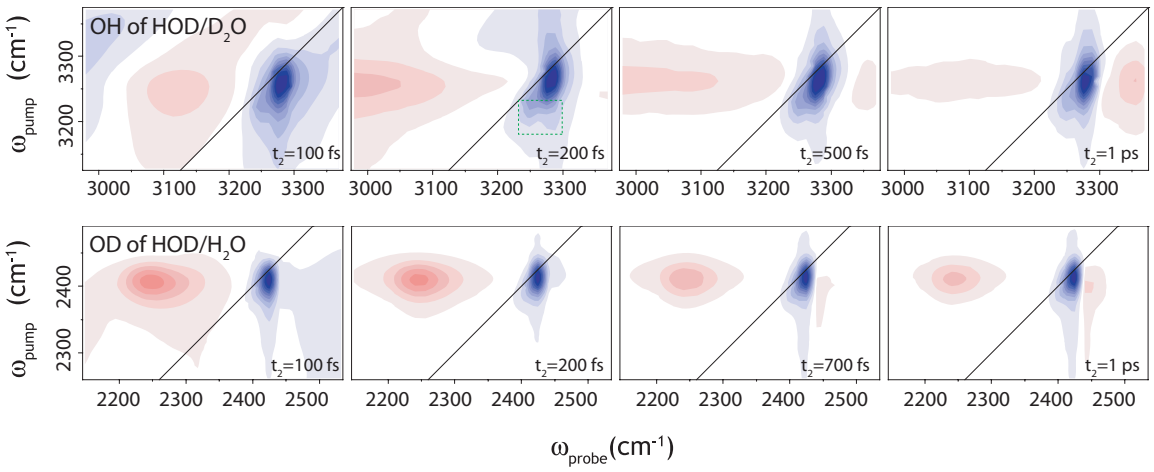


FIG. 2. Experimental purely absorptive 2D IR spectra of the OH stretch of HOD/$D_2O$ (upper row) and of the OD stretch of HOD/$H_2O$ (lower row) at $T = 80K$ for different population times $t_2$. In both cases, a very broad excited state signal (red lobe) in comparison to that associated with ground state processes (blue lobe) is observed. The lineshape of the ground state exhibits surprisingly little inhomogeneity due to proton disorder (substructure in the green square) as discussed in the text.

in hydrogen bond strengths. Apparently, proton disorder in ice Ih affects the hydrogen bond strength of the vibrational chromophores too little to cause appreciable inhomogeneous broadening. The bands appear to be mostly homogeneously broadened, probably due to fast thermal fluctuations.

Finally, at late population times (1 ps), a positive (red) contribution at higher frequencies is observed for both isotope mixtures (Fig. 2). This effect has also been observed by pump-probe spectroscopy of OH of HOD/$D_2O$,[39] as a growing contribution of a 400 fs timescale at 3380 $cm^{-1}$, in agreement with our observations. The appearance of this band has been attributed to the vibrational relaxation through an intermediate state likely related to bending mode and intermolecular relaxation.

Figure 3 focuses on the dynamics of the 0-1 and 1-2 transitions for both isotopic mixtures. Plotted is the signal intensity of the center of the blue and red lobes of the 2D IR spectra as a function of population time $t_2$. The signal decays due to vibrational relaxation, and in addition, quantum beats are observed for the OH stretch vibration of HOD/$D_2O$ [Fig. 3(a)]. The solid lines are fits using the following function:

$$S(t) = A_1 \cdot e^{-t/\tau_1} + A_2 \cdot e^{-t/\tau_2} \cdot \cos\left(\frac{2\pi t}{\tau_3} + \phi\right), \quad (2)$$

where $A_1$ and $A_2$ are the amplitudes of the exponential decay and the oscillatory component, $\tau_1$ is the signal decay time constant, $\tau_2$ the oscillatory component time constant and $\tau_3$ the oscillation period and $\phi$ the phase. For the OH vibration of HOD/$D_2O$ [Fig. 3(a)], we observe a close to exponential decay, with time constants of (590 ± 60) fs for the 0-1 transition (blue circles) and (440 ± 50) fs for the 1-2 transition, in agreement with previous studies.[38,39] In addition, a damped oscillatory contribution is observed with frequency (150 ± 10) $cm^{-1}$ and amplitude $A_2 = 50\%\ A_1$. Beating is not evident within the signal-to-noise ratio for the OD case, which exhibits a decay time constant of (410 ± 20) fs for the 0-1 (blue circles) transition and (360 ± 40) fs for the 1-2 transition.

## IV. THEORY

The two features in the 2D IR response that need to be explained are (a) the quantum beats observed for the OH vibration of HOD/$D_2O$, as well as (b) the asymmetry in the width of lineshapes of the 0-1 transition *versus* the 1-2 transition. The latter is extremely pronounced for the OH vibration of HOD/$D_2O$ (and has also been observed in IR pump-probe spectroscopy[38,39]) but is still very significant for the OD vibration of HOD/$H_2O$. In the following, we will

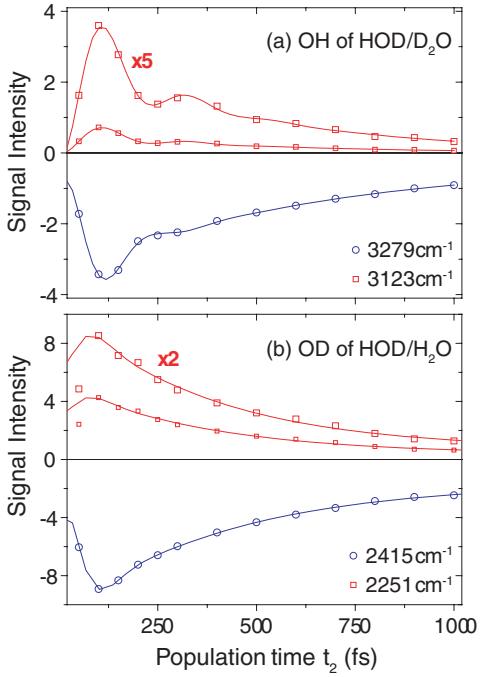


FIG. 3. Dynamics of the 0-1 (blue circles) and 1-2 transitions (small red squares) extracted for the experimental 2D IR spectra for the (a) OH stretch vibration of HOD/$H_2O$ and (b) for the OD stretch vibration of HOD/$D_2O$. The signal of the 1-2 transition is scaled up by factors 5 and 2, respectively (large red squares). The sold lines represent exponential fits, in the OH case with a damped oscillatory component included.

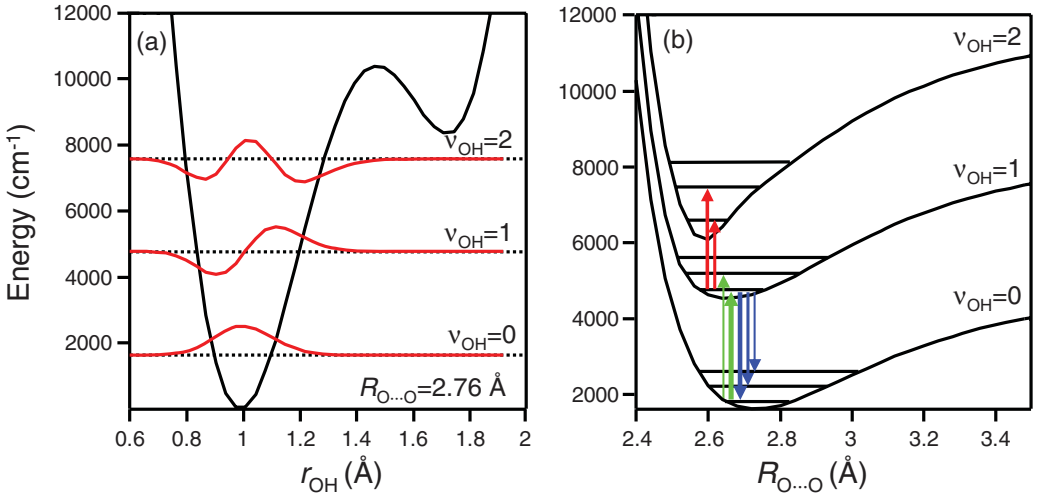


FIG. 4. Adiabatic representation of the Lippincott-Schroeder model for the OH vibration of HOD/$D_2O$, using the same parameters as in Figs. 5 and 6. (a) A cut through the Lippincott-Schroeder potential for $R_{O\cdots O}$ =2.76 Å, the hydrogen bond distance in ice Ih. The eigenstates corresponding to the OH-stretch vibrations are shown. (b) The dependence of the OH-stretch energies in dependence of the hydrogen bond length $R_{O\cdots O}$. The most important Franck-Condon like transitions are shown in the same color code as in Fig. 5: bleach in green, stimulated emission in blue, and excited state absorption in red.

apply the Lippincott-Schroeder[43,44] model to qualitatively explain these features. The Lippincott-Schroeder model is a one-dimensional model of the hydrogen bond including two most relevant degrees of freedom, i.e., the O-H (or O-D) bond length $r_{OH}$ and the O···O hydrogen bond length $R_{O\cdots O}$. These two degrees of freedom are extremely strongly coupled, much stronger than, for example, to the hydrogen bond bending coordinate.[52] We use the functional form:

$$V(r, R) = V_{Ia} + V_{Ib} + V_{II}, \tag{3}$$

with

$$\begin{aligned} V_{Ia} &= D_{Ia}[1 - e^{-n_{Ia}(r_{OH}-r_0)^2/2r_{OH}}], \\ V_{Ib} &= D_{Ib}[1 - e^{-n_{Ib}(R_{O\cdots O}-r_{OH}-r_0)^2/2(R_{O\cdots O}-r_{OH})}], \\ V_{II} &= D_{II}[1 - e^{-n_{II}(R_{O\cdots O}-R_0)}]^2, \end{aligned} \tag{4}$$

where $r_{OH}$ is the gas phase O-H (or O-D) bond length. The ansatz takes the point of view that the proton is bound to the one oxygen through term $V_{Ia}$ with a binding energy $D_{Ia}$, but can in principle also bind to the other oxygen with binding energy $D_{Ib}$ (which is assumed to be smaller since proton transfer is asymmetric in this case). Furthermore, both oxygens interact through a Morse potential $V_{II}$ with an equilibrium distance determined by $R_0$. The Lippincott-Schroeder potential is phenomenological but *ab-initio* calculation have verified its essential features.[63]

The Lippincott-Schroeder model was originally designed to explain the energetics and spectroscopy of hydrogen bonded crystals, in particular the strong dependence of the OH vibrational frequency on the O···O hydrogen bond length.[43,44] Bakker and co-workers have extended the idea and applied it to pump-probe spectroscopy, which, in essence, includes higher vibrational states. They explain successfully the asymmetry of the spectral width of the 0-1 versus the 1-2 transition in the IR-pump-probe response in liquid water,[50,51] but conclude that it fails for ice Ih,[39] where this asymmetry is much more pronounced but structural disorder is less. We show here that we can in fact explain the 2D IR response of both the OH vibration of HOD/$D_2O$ and the OD vibration of HOD/$H_2O$, when taking into account non-adiabatic couplings within the Lippincott-Schroeder potential.

The Lippincott-Schroeder model is of course very idealized when studying ice. First, it reduces the problem to that of a water-dimer, whereas in reality water molecules vibrate against each other in longitudinal acoustic or optical phonons. Furthermore, the Lippincott-Schroeder potential is dissociative along the $R_{O\cdots O}$ coordinate with a continuum of states above essentially $D_{II}$, which is not realistic in the crystal due to cage effects. On the other hand, due the finite grid in the numerical diagonalization of the Hamiltonian, the O···O hydrogen bond length is in fact confined as well, albeit in a very artificial manner (essentially like a particle-in-the-box problem). Overall, we do *not* consider the outcome of the Lippincott-Schroeder model to be quantitative. In particular, we did *not* attempt to fit parameters to the experimental results since we feel that this would take the model too far. Nevertheless, the Lippincott-Schroeder model captures in essence the large anharmonic coupling between the two degrees of freedom, so it is worthwhile exploring what are the model's predictions for 2D IR spectroscopy. In a more realistic modeling, one might perform a mixed-quantum-classical simulation, treating the HOD···$OH_2$ quantum-mechanically and the remainder of the crystal as classical bath. While such a simulation would definitively be very illustrative, it goes beyond the scope of this paper.

Figure 4 shows the usual adiabatic treatment of the Lippincott-Schroeder potential. One first solves the 1D $r_{OH}$-Schrödinger equation for a given hydrogen bond distance $R_{O\cdots O}$ (2.76 Å in Fig. 4(a), which is the hydrogen bond distance in ice Ih[15]) revealing adiabatic states for the OH stretch vibration. Repeating this for all $R_{O\cdots O}$'s, one assembles "potential energy surfaces" for each $\nu_{OH}$ stretch state [Fig. 4(b), note that all this is on an electronic ground-state

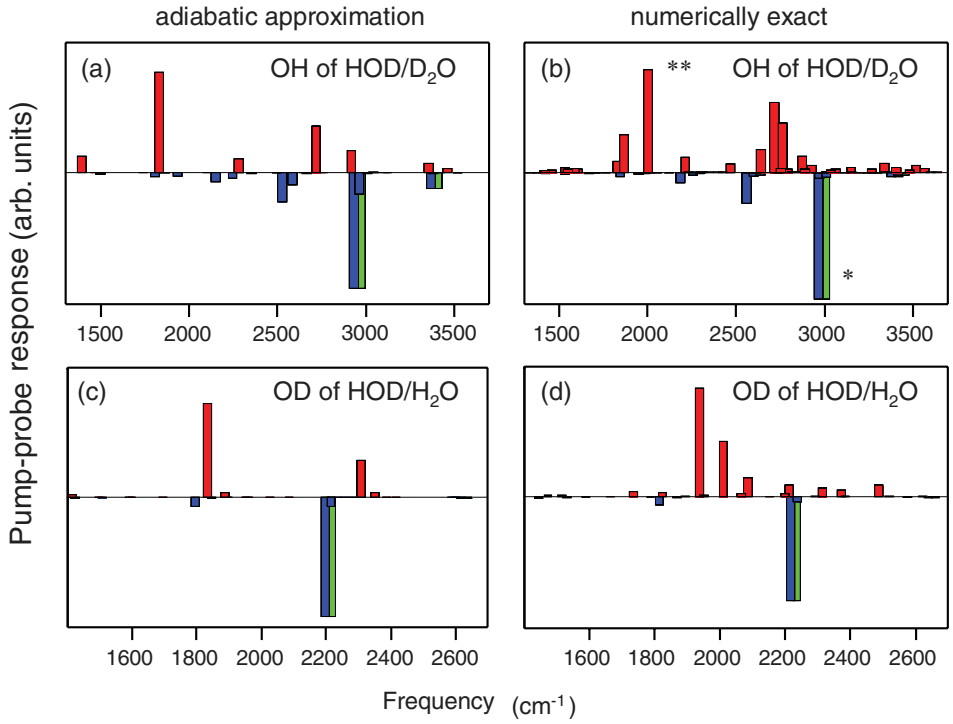


FIG. 5. Simulated incoherent pump-probe response for (a, b) the OH vibration of HOD in $D_2O$ and (c, d) the OD vibration of HOD in $H_2O$. Panel (a, c) treat the problem in the adiabatic approximation, and (b, d) on a numerically exact level. Green depict bleach signals, blue stimulated emission signals and red excited state absorption signals [i.e., sam color code as in Fig. 4(b)]. The bleach signals are artificially shifted somewhat to higher frequencies so that they are visible next to the overlapping stimulated emission lines. The asterisks "*" and "**" label transitions to the wavefunctions shown in Figs. 6(c) and 6(d), respectively.

surface]. Finally, the $R_{O\cdots O}$-motion is quantized on these surfaces. This leads to Franck-Condon like transitions with the corresponding progressions, just like in electronic (vibronic) spectroscopy.

Figures 5(a) and 5(c) shows a simulated incoherent IR pump-probe spectrum (see Material and Methods). We discriminate bleach signals (green), stimulated emission signals (blue) and excited state absorption signals (red), following the colorcode of Fig. 4(b). The bleach signal mirrors a linear absorption spectrum (squared) with the dominating zero-phonon line at about 3000 $cm^{-1}$ (for OH in $HOD/D_2O$) and a small progression band at about 3400 $cm^{-1}$. The stimulated emission signal includes an additional Franck Condon progression towards lower frequencies, which originates mostly from the transition from $\nu_{O\cdots O} = 0$ in the OH first excited states $\nu_{OH} = 1$ down to several quanta in the O···O coordinate in the OH ground state $\nu_{OH} = 0$. The progression of the stimulated emission towards lower frequencies is more pronounced than that of the bleach, since the former scales with the square of the transition dipoles (Franck-Condon factors) and the latter with the fourth power. In addition, we find excited state absorption bands over a wide frequency range. The corresponding Franck-Condon progressions are not regular due to the strong anharmonic character of the adiabatic potential energy surfaces and also their different energy spacings.

In order to test the quality of the adiabatic approximation, we also solve the 2D Schrödinger equation on a numerically exact level, which implicitly includes non-adiabatic coupling between the various $\nu_{OH}$-stretch states. Figure 6 shows some examples of vibrational wavefunctions, e.g., the ground state in Fig. 6(a) and the first excited state with respect to the O···O hydrogen bond coordinate in Fig. 6(b) (its vibrational frequency, 405 $cm^{-1}$, overestimates the experimentally observed value by a factor of 2-3). The perpendicular nodal plane of the wavefunction in Fig. 6(c) indicates that this is the first excited state with respect to the OH stretch coordinate. However, clearly some weak mode-mixing appears with a state that contains many quanta in the O···O hydrogen bond vibration (from the build up of O···O states in the energy range around this eigenstate, we conclude that it is the 13th excited state). Hence, the state could be approximated as $\Psi = c_1|1_{OH}\rangle|0_{O\cdots O}\rangle + c_2|0_{OH}\rangle|13_{O\cdots O}\rangle$ with $c_2 \ll c_1$, where $|i_{OH}\rangle$ and $|i_{O\cdots O}\rangle$ are states with $i$ quanta in the $r_{OH}$ or the $R_{O\cdots O}$ coordinates, respectively. Mode mixing in the $\nu_{OH} = 2$ manifold becomes severely stronger and a clear assignment of these states is no longer possible [Fig. 6(d)].

In Fig. 5(b) is presented the resulting pump-probe spectrum. The appearance of bleach and stimulated emission signals can perfectly be understood in the framework of the adiabatic representation (Fig. 4). Due to the strong mode mixing at higher energies, however, the adiabatic representation breaks down for the excited state absorption signals [Fig. 5(b), red]. The state shown in Fig. 6(d) is the one which gives rise to the strongest transition in the excited state absorption spectrum [marked with "**" in Fig. 5(b)], but many other states carry oscillator strength as well. Due to non-adiabatic coupling, the various Franck-Condon transitions into the $\nu_{OH} = 2$ manifold couple with a quasi-continuum of states from $\nu_{OH} = 0$ and $\nu_{OH} = 1$, so they spread out and we get an

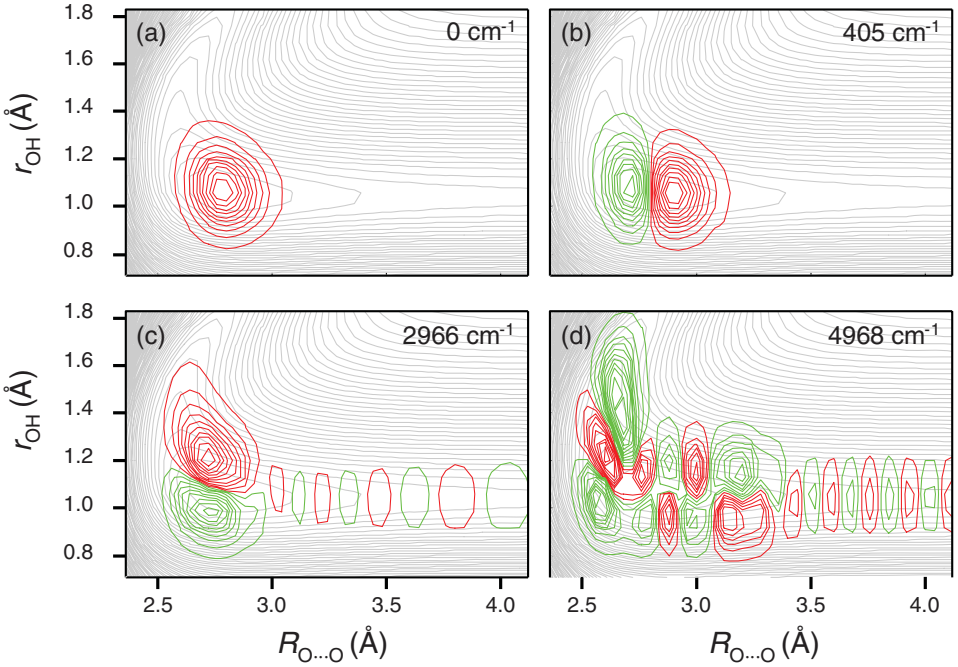


FIG. 6. Full 2D vibrational wavefunctions in the Lippincott-Schroeder potential for the OH vibrations of HOD in $D_2O$ together with their energies. Shown are (a) the ground state and excited states with (b) one quantum in the O···O hydrogen bond coordinate, (c) one quantum in the OH-coordinate $\nu_{OH} = 1$, and (d) two quanta in the OH-coordinate $\nu_{OH} = 2$. The states in panel (c, d) are those that give rise to the transitions depicted by "*" and "**" in Fig. 5(b), respectively. The grey contour lines in the background depict the potential energy surface (contour line spacing 1000 $cm^{-1}$). The energies do not include zero-point energy of 1835 $cm^{-1}$.

irregular pattern of excited state transitions that extends over more than 2000 $cm^{-1}$. For the OD case, this effect is significantly reduced, but still present [Fig. 5(d)].

Figure 7 shows simulated 2D IR spectra in dependence of the population time $t_2$, and Fig. 8 the time dependence of the intensity of the peaks marked by an asterisk in Fig. 7. The later is to be compared with the experimental data in Fig. 3 (red curves). In particular, the excited state contribution strongly beats for the OH vibration of $HOD/D_2O$ with an oscillation period of ≈550 $cm^{-1}$ (we note again that the Lippincott-Schroeder potential we used overestimates the hydrogen-bond vibration frequency). Owing to the anharmonicity of the $\nu_{OH} = 1$ potential energy surface, these beats dephase after about 450 fs (Fig. 8) as the wavefunction disperses (the wavepacket again rephases at longer $t_2$-times). Quantum beating is significantly less for the OD vibration of $HOD/H_2O$ (Fig. 8, blue line). Due to the lower energy regime reached in this case, less of the anharmonicity of the Lippincott-Schroeder potential is explored, so the adiabatic potentially energy surfaces [i.e., the equivalent of Fig. 4(b)] are less displaced and the wavepacket is less oscillatory.

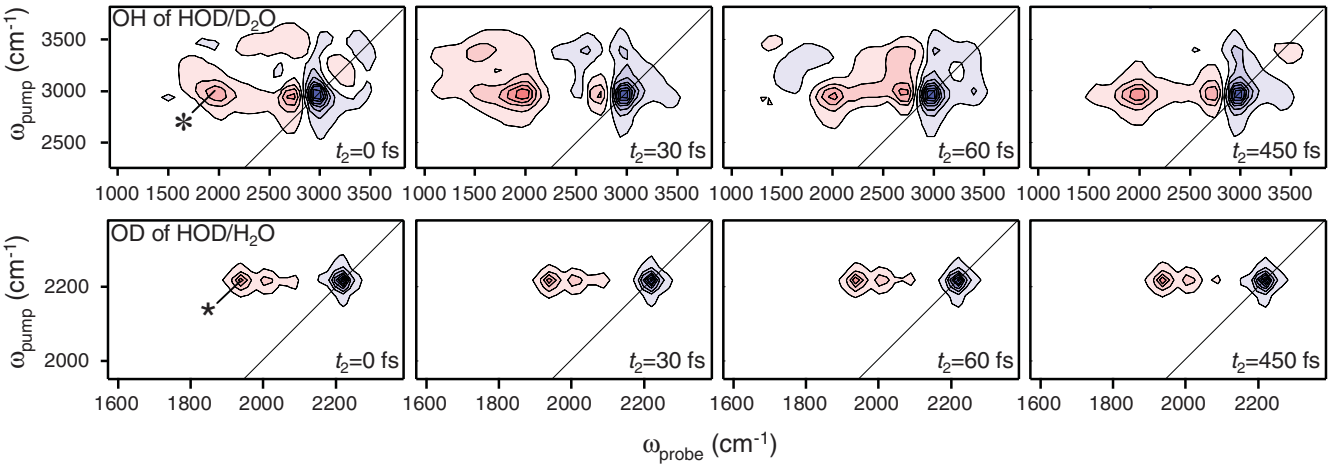


FIG. 7. Simulated purely-absorptive 2D IR spectra for the OH vibration of $HOD/D_2O$ (top row) and the OD vibration of $HOD/H_2O$ (bottom row) for various population times $t_2 = 0$ fs, $t_2 = 30$ fs, $t_2 = 60$ fs, and $t_2 = 450$ fs (when most of the quantum coherence is dephased). The asterisk (*) marks the positions, whose time-dependence is depicted in Fig. 8.

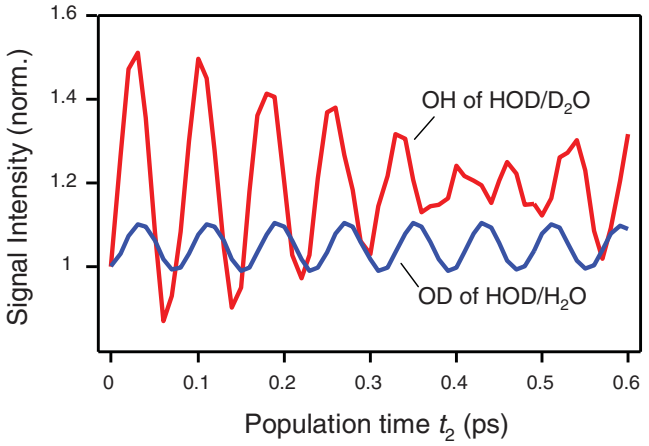


FIG. 8. Time-dependence of the intensity of the 2D IR peaks marked by an asterisk (*) in Fig. 7. Red: OH vibration of HOD/$D_2O$, blue: OD vibration of HOD/$H_2O$.

## V. DISCUSSION AND CONCLUSIONS

We performed 2D IR measurements of isotope diluted ice Ih for both the OH vibration in HOD/$D_2O$ and the OD vibration of HOD/$H_2O$ at 80 K. Based on the Lippincott-Schroeder model, we attempt to reproduce our observations and to understand the physical mechanisms behind these processes. Despite the conceptual crudeness of the Lippincott-Schroeder model (i.e., restriction to two degrees of freedom, treatment as a water-dimer), semi-quantitative agreement with the experimental observations is obtained.

We observe a significantly broader excited state absorption signal than that of the bleach and the stimulated emission, in agreement with previous pump-probe measurements of the OH stretch vibration of HOD/$D_2O$.[38,39] Bakker and co-workers explained the broad linewidth of the 1-2 transition by lifetime broadening caused by a Fermi resonance with the first overtone of the HOD bending vibration.[39] The observation of the same effect for the OD vibration of HOD/$H_2O$, however, suggests the presence of an alternative mechanism, since the overtone of the HOD bending is no longer in resonance. Non-adiabatic treatment of the Lippincott-Schroeder model can explain the effect for both the OH and the OD vibration, including the less pronounced broadening in the OD case, since non-adiabatic coupling will also lead to efficient de-excitation of the $\nu_{OH} = 2$ state. Bakker and co-workers used the same Lippincott-Schroeder model with the same set of parameters when they concluded that it cannot explain the asymmetry in linewidth.[39] However, they argued in terms of a classical distribution of O···O distances, which for ice Ih is too small to explain the effect (in contrast to liquid water[50,51]). In essence, it is the quantum-mechanical delocalization of the wavefunction in the $R_{O\cdots O}$ direction (Fig. 6), which effectively causes a wide range of O···O distances and hence Franck-Condon like transitions in a wide range of frequencies. The quantum-mechanical nature of the O···O coordinate has been neglected in Ref. 39.

Quantum beats are observed both in the experiment and theory, which represent a coherent oscillation of the O···O hydrogen bond degree of freedom. In the framework of the adiabatic picture shown in Fig. 4, these quantum beats are understood as O···O wavepackets that are generated after impulsive excitation into the displaced $\nu_{OH} = 1$ potential energy surface. In our simulations, the wavepacket dephases after ≈450 fs, since the $\nu_{OH} = 1$ potential energy surface is anharmonic, with recurrences that appear afterwards. In reality, however, dephasing is irreversible (i.e., nonrecurrent), possibly due to thermal fluctuations and potentially also due to the inhomogeneity caused by proton disorder. Hardly any quantum beating is found for the OD stretch vibration in HOD/$H_2O$, since anharmonicity of the potential energy surface is less pronounced at the lower energy of the OD excitation. The beating frequency provides information concerning the nature of these intermolecular modes. A band at 156 $cm^{-1}$ in the low frequency IR spectrum of isotope dilute ice $H_2O/D_2O$ was assigned to longitudinal acoustic (LA) phonons at the boundary of the Brillouin zone.[29] The mechanism of the coherent excitation of such zone boundary phonons likely is the same as after electronic excitations of diatomic molecules (e.g., $Br_2$, $I_2$) in rare gas matrices.[64] Also a mixed quantum-classical MD simulation of ice Ih (i.e., treating the OH or OD vibrator quantum-mechanically but the lattice motion as classical) revealed an oscillatory response in the frequency fluctuation correlation function of the OH vibration with a frequency of 230 $cm^{-1}$ (in fair agreement with the experimentally observed beating frequency of 150 ±10 $cm^{-1}$), which was assigned to the intermolecular hydrogen bond stretch coordinate.[22] We conclude that the experimentally observed beats reflect the same mode.

We hardly resolve any signature of inhomogeneous broadening in the 2D-IR spectra. In Ref. 22, it has been concluded based on MD simulations that proton disorder leads to an inhomogeneous broadening of ≈70 $cm^{-1}$. However, as also mentioned in Ref. 22, this width overestimates the experimentally observed total width of 25 $cm^{-1}$ at 10 K significantly.[33] Given the complication in the interpretation of the 2D IR lineshape that arises from the coupling to the O···O mode, the quantum-mechanical character of which is not included in the simulation of Ref. 22, we cannot exclude an inhomogeneous distribution on the order of 25 $cm^{-1}$.

It is illustrative to compare the 2D IR response of ice Ih with that of liquid water.[59–62] Also in liquid water, the 1-2 transition is broader than the 0-1 transition, and in fact it has been argued that this reflects the anharmonic coupling to the O···O hydrogen the bond length.[50,51] However, due to the much larger effect of disorder in water, this effect is largely blurred. Hence it appears that ice Ih is better suited to study the quantum-mechanical character of the hydrogen bond and its consequence for vibrational spectroscopy. Beatings have also been observed in the frequency fluctuation correlation function of liquid water by photon echo spectroscopy,[65] as well as theoretically.[66,67] The frequency is comparable (180 $cm^{-1}$), and it is also assigned to an slightly underdamped oscillatory motion of the intermolecular hydrogen bond coordinate. Not surprisingly, the oscillatory contribution is damped less in the crystalline state. Finally, conformational disorder in liquid water leads to a measurable tilt in the 2D IR lineshapes,[59–62] whereas proton disorder in ice Ih has a very small effect on the OH stretch frequency to be detected.

There has been a long standing debate concerning the lineshape of neat ($H_2O$ and $D_2O$) ice Ih,[23,28,68] which exhibits much more complex structure than that of isotope diluted ice Ih. One explanation of the complex linear spectra is based on the strong excitonic coupling between individual water molecules.[23] In this context, an extension of the current work to neat $H_2O$ and $D_2O$ ice Ih will be interesting, since the appearance of cross peaks in 2D IR spectroscopy report on exciton coupling. We will discuss such experiments in a future publication.

## ACKNOWLEDGMENTS

This work has been initiated by an inspiring discussion with Jim Skinner. We would like to thank Jan Helbing, Julien Rehault and Mathias Hausherr for their continuous help in the lab, as well as to Gerhard Stock and Sean Garrett-Roe for valuable discussions and comments. This work was supported by the Swiss National Science Foundation (SNF) through the NCCR MUST.

[1] J. Swenson, H. Jansson, J. Hedström, and R. Bergman, J. Phys.: Condens. Matter **19**, 205109 (2007).
[2] M. Arakawa, H. Kagi, and H. Fukazawa, Astrophys. J., Suppl. Ser. **184**, 361 (2009).
[3] L. Decin, M. Agúndez, M. J. Barlow, F. Daniel, J. Cernicharo, R. Lombaert, E. De Beck, P. Royer, B. Vandenbussche, R. Wesson, E. T. Polehampton, J. A. D. L. Blommaert, W. De Meester, K. Exter, H. Feuchtgruber, W. K. Gear, H. L. Gomez, M. A. T. Groenewegen, M. Guélin, P. C. Hargrave, R. Huygen, P. Imhof, R. J. Ivison, C. Jean, C. Kahane, F. Kerschbaum, S. J. Leeks, T. Lim, M. Matsuura, G. Olofsson, T. Posch, S. Regibo, G. Savini, B. Sibthorpe, B. M. Swinyard, J. A. Yates, and C. Waelkens, Nature (London) **467**, 64 (2010).
[4] P. Ball, Nature (London) **452**, 291 (2008).
[5] P. Wernet, D. Nordlund, U. Bergmann, M. Cavalleri, M. Odelius, H. Ogasawara, L. Å. Näslund, T. K. Hirsch, L. Ojamäe, P. Glatzel, L. G. M. Pettersson, and A. Nilsson, Science **304**, 995 (2004).
[6] N. Bjerrum, Science **115**, 385 (1952).
[7] F. H. Stillinger, Science **209**, 451 (1980).
[8] C. Huang, K. T. Wikfeldt, T. Tokushima, D. Nordlund, Y. Harada, U. Bergmann, M. Niebuhr, T. M. Weiss, Y. Horikawa, M. Leetmaa, M. P. Ljungberg, O. Takahashi, A. Lenz, L. Ojamäe, A. P. Lyubartsev, S. Shin, L. G. M. Pettersson, and A. Nilsson, Proc. Natl. Acad. Sci. U.S.A. **106**, 15214 (2009).
[9] G. N. I. Clark, G. L. Hura, J. Teixeira, A. K. Soper, and T. Head-Gordon, Proc. Natl. Acad. Sci. USA **107**, 14003 (2010).
[10] S. Garrett-Roe and P. Hamm, Phys. Chem. Chem. Phys. **12**, 11263 (2010).
[11] D. D. Klug, Nature (London) **420**, 749 (2002).
[12] E. A. Zheligovskaya and G. G. Malenkov, Russ. Chem. Rev. **75**, 57 (2006).
[13] C. G. Salzmann, P. G. Radaelli, E. Mayer, and J. L. Finney, Phys. Rev. Lett. **103**, 105701 (2009).
[14] T. Loerting and N. Giovambattista, J. Phys.: Condens. Matter **18**, R919 (2006).
[15] J. D. Bernal and R. H. Fowler, J. Chem. Phys. **1**, 515 (1933).
[16] L. Pauling, J. Am. Chem. Soc. **57**, 2680 (1935).
[17] S. W. Rick, J. Chem. Phys. **122**, 094504 (2005).
[18] H. Fukazawa, S. Ikeda, and S. Mae, Chem. Phys. Lett. **282**, 215 (1998).
[19] H. Fukazawa, S. Ikeda, M. Oguro, T. Fukumura, and S. Mae, J. Phys. Chem. B **106**, 6021 (2002).
[20] S. J. Singer, J. Kuo, T. K. Hirsch, C. Knight, L. Ojamäe, and M. L. Klein, Phys. Rev. Lett. **94**, 135701 (2005).
[21] Y. O. K. Abe and T. Shigenari, *Physics and Chemistry of ice* (Royal Society of Chemistry, London, 2006).
[22] F. Li and J. L. Skinner, J. Chem. Phys. **132**, 204505 (2010).
[23] F. Li and J. L. Skinner, J. Chem. Phys. **133**, 244504 (2010).
[24] H. J. Prask, J. Chem. Phys. **56**, 3217 (1972).
[25] W. F. Kuhs and M. S. Lehmann, J. Phys. Chem. **87**, 4312 (1983).
[26] J. C. Li, D. Londono, D. K. Ross, J. L. Finney, S. M. Bennington, and A. D. Taylor, J. Phys.: Condens. Matter **4**, 2109 (1992).
[27] L. E. Bove, S. Klotz, A. Paciaroni, and F. Sacchetti, Phys. Rev. Lett. **103**, 165901 (2009).
[28] J. E. Bertie and E. Whalley, J. Chem. Phys. **40**, 1637 (1964).
[29] J. E. Bertie, J. Chem. Phys. **46**, 1271 (1967).
[30] J. R. Scherer and R. G. Snyder, J. Chem. Phys. **67**, 4794 (1977).
[31] E. Whalley, Can. J. Chem. **55**, 3429 (1977).
[32] M. S. Bergren, D. Schuh, M. G. Sceats, and S. A. Rice, J. Chem. Phys. **69**, 3477 (1978).
[33] T. C. Sivarkumar, S. A. Rice, and M. G. Sceats, J. Chem. Phys. **69**, 3468 (1978).
[34] H. Iglev, M. Schmeisser, Simeonidis, A. Thaller, and A. Laubereau1, Nature (London) **439**, 183 (2006).
[35] G. C. Pimentel and A. McClellan, *The Hydrogen Bond* (Freeman, San Francisco, CA, 1960).
[36] S. A. Corcelli and J. L. Skinner, J. Phys. Chem. A **109**, 6154 (2005).
[37] S. Mukamel, *Principles of Nonlinear Optical Spectroscopy* (Oxford University Press, Oxford, 1995).
[38] G. Seifert, K. Weidlich, and H. Graener, Phys. Rev. B **56**, R14231 (1997).
[39] A. M. Dokter and H. J. Bakker, J. Chem. Phys. **128**, 024502 (2008).
[40] S. Woutersen, U. Emmerichs, H. Nienhuys, and H. J. Bakker, Phys. Rev. Lett. **81**, 1106 (1998).
[41] R. L.A. Timmer and H. J. Bakker, J. Phys. Chem. A **114**, 4148 (2010).
[42] A. M. Dokter, C. Petersen, S. Woutersen, and H. J. Bakker, J. Chem. Phys. **128**, 044509 (2008).
[43] E. R. Lippincott and R. Schroeder, J. Chem. Phys. **23**, 1099 (1955).
[44] R. Schroeder and E. R. Lippincott, J. Phys. Chem. **61**, 921 (1957).
[45] P. Hamm, R. A. Kaindl, and J. Stenger, Opt. Lett. **25**, 1798 (2000).
[46] N. Demirdoven, M. Khalil, O. Golonzka, and A. Tokmakoff, Opt. Lett. **27**, 433 (2002).
[47] L. P. DeFlores, R. A. Nicodemus, and A. Tokmakoff, Opt. Lett. **32**, 2966 (2007).
[48] J. Helbing and P. Hamm, J. Opt. Soc. Am. B **28**, 171 (2011).
[49] R. Bloem, S. Garrett-Roe, H. Strzalka, P. Hamm, and P. Donaldson, Opt. Express **18**, 27067 (2010).
[50] H. J. Bakker and H. K. Nienhuys, Science **297**, 587 (2002).
[51] H. J. Bakker, H. K. Nienhuys, G. Gallot, N. Lascoux, G. M. Gale, J. C. Leiknam, and S. Bratos, J. Chem. Phys. **116**, 2592 (2002).
[52] A. Staib and J. T. Hynes, Chem. Phys. Lett. **204**, 197 (1993).
[53] T. Saitoh, K. Mori, and R. Itoh, Chem. Phys. **60**, 161 (1981).
[54] K. Ando, J. Chem. Phys. **125**, 014104 (2006).
[55] G. C. Groeneboom and D. T. Colbert, J. Chem. Phys. **99**, 9681 (1993).
[56] P. Hamm and M. T. Zanni, *Concepts and Methods of 2D Infrared Spectroscopy* (Cambridge University Press, Cambridge, 2011).
[57] K. Ohno, M. Okimura, N. Akai, and Y. Katsumoto, Phys. Chem. Chem. Phys. **7**, 3005 (2005).
[58] J. Max and C. Chapados, J. Chem. Phys. **116**, 4626 (2002).
[59] J. B. Asbury, T. Steinel, K. Kwak, S. A. Corcelli, C. P. Lawrence, J. L. Skinner, and M. Fayer, J. Chem. Phys. **121**, 12431 (2004).
[60] S. Yeremenko, M. S. Pshenichnikov, and D. A. Wiersma, Chem. Phys. Lett. **369**, 107 (2003).
[61] J. D. Eaves, J. J. Loparo, C. J. Fecko, S. T. Roberts, A. Tokmakoff, and P. L. Geissler, Proc. Natl. Acad. Sci. USA **102**, 13019 (2005).
[62] F. Perakis and P. Hamm, "Two-dimensional infrared spectroscopy of supercooled water," J. Phys. Chem. B (in press).
[63] M. V. Vener, Chem. Phys. Lett. **244**, 89 (1995).
[64] M. Gühr and N. Schwentner, Phys. Chem. Chem. Phys. **7**, 760 (2005).
[65] C. J. Fecko, J. D. Eaves, J. J. Loparo, A. Tokmakoff, and P. L. Geissler, Science **301**, 1698 (2003).
[66] C. P. Lawrence and J. L. Skinner, J. Chem. Phys. **117**, 8847 (2002).
[67] K. B. Moller, R. Rey, and J. T. Hynes, J. Phys. Chem. A **108**, 1275 (2004).
[68] V. Buch and J. P. Devlin, J. Chem. Phys. **110**, 3437 (1999).